Modulation of phosphatidylinositol 4-phosphate levels by CaBP7 controls cytokinesis in mammalian cells

Dayani Rajamanoharan, Hannah V. McCue, Robert D. Burgoyne, and Lee P. Haynes
Department of Cellular and Molecular Physiology, Institute of Translational Medicine, University of Liverpool, Liverpool L69 3BX, United Kingdom

ABSTRACT Calcium and phosphoinositide signaling regulate cell division in model systems, but their significance in mammalian cells is unclear. Calcium-binding protein-7 (CaBP7) is a phosphatidylinositol 4-kinaseIIIβ (PI4KIIIβ) inhibitor required during cytokinesis in mammalian cells, hinting at a link between these pathways. Here we characterize a novel association of CaBP7 with lysosomes that cluster at the intercellular bridge during cytokinesis in HeLa cells. We show that CaBP7 regulates lysosome clustering and that PI4KIIIβ is essential for normal cytokinesis. CaBP7 depletion induces lysosome mislocalization, extension of intercellular bridge lifetime, and cytokinesis failure. These data connect phosphoinositide and calcium pathways to lysosome localization and normal cytokinesis in mammalian cells.

INTRODUCTION

Phosphoinositides (PIs) constitute <1% of cellular lipid in mammalian cells but are important mediators of many signaling pathways (Balla, 2013). Phosphatidylinositiol 4-phosphate (PI4P), one of seven possible PIs, can exert biological effects through either induction of local membrane curvature (Furse et al., 2012; important for transport vesicle biogenesis) or recruitment of signaling proteins harboring PI4P-selective binding domains (Lenoir and Overduin, 2013).

Golgi-localized PI4KIIIβ is the most extensively studied PI4K isoform and, along with its yeast homologue pik1, functions in secretory cargo trafficking from the trans-Golgi network (TGN; Walch-Solimena and Novick, 1999; Haynes et al., 2005). PI4KIIIβ is a soluble enzyme recruited to the TGN by the small GTPase ADP-ribosylation factor 1 (ARF1; Godi et al., 1999). ARF1 activates PI4KIIIβ to drive PI4P production and biogenesis of secretory vesicles. PI4KIIIβ regulation at the TGN in mammalian cells is further influenced by two Ca^{2+}-binding proteins, neuronal calcium sensor-1 (NCS-1; a Ca^{2+}-dependent

activator) and CaBP7 (a Ca^{2+}-independent inhibitor; Zhao et al., 2001; Haynes et al., 2005; Mikhaylova et al., 2009).

CaBP7 is an EF-hand containing, Ca^{2+}-binding protein (McCue et al., 2010a,b, 2012). It is involved in the biogenesis of vesicular carriers from the TGN in neuronal cells, consistent with its function as a PI4KIIIβ regulator (Mikhaylova et al., 2009). CaBP7 also appears to regulate cytokinesis in mammalian cells (Neumann et al., 2010), although how it achieves this remains to be determined. Cytokinesis is fundamental for normal cellular growth, development, and aging. Defects in this process can ultimately lead to a state of aneuploidy and cellular transformation (Ly et al., 2000; Baker et al., 2005; Pfau and Amon, 2012; Ricke and van Deursen, 2013).

Studies in model organisms have demonstrated PI4KIIIβ activity is important during cytokinesis (Polevoy et al., 2009; Brill et al., 2011; Echard, 2012). Evidence that PI4P is required during mitosis in mammalian cells derives from studies examining knockdown of the sole PI4P phosphatase, Sac1. Sac1 depletion in HeLa cells disrupts Golgi morphology and generates mitotic spindle defects (Liu et al., 2008). PI4P is an important factor during mitosis, and evidence from nonmammalian systems indicates that PI4KIIIβ may be the enzyme regulating its production.

Recently it was reported that a pool of PI4KIIIβ localizes to lysosomes (Sridhar et al., 2013). Lysosomes were long considered a terminal destination of the secretory pathway where cellular material consigned for recycling was trafficked. Accumulating evidence suggests that these organelles have additional, nondegradative, functions, including acting as Ca^{2+}-signaling platforms (Galione et al., 2010; McCue et al., 2013) and as lipid reservoirs during membrane repair events (Holt et al., 2006; Luzio et al., 2007b).

In this article, we show that CaBP7 undergoes a cell cycle–dependent redistribution from the Golgi apparatus at interphase to lysosomes during mitosis and to a mixed Golgi/lysosomal localization at cytokinesis. We report that lysosomes positive for CaBP7 cluster to either side of the intercellular bridge during cytokinesis and that CaBP7 depletion blocks both this clustering and the final abscission step to generate aneuploid cells. More specifically, CaBP7 loss of function appears to extend intercellular bridge lifetime, leading to abscission failure as determined in time-resolved live-cell imaging experiments. Cytokinesis is also inhibited by overexpression of wild-type PI4KIIIβ and by the PI4KIIIβ activators ARF1 and NCS-1 but not by overexpression of wild-type CaBP7 or a catalytically inactive version of PI4KIIIβ. This is the first demonstration that PI4KIIIβ activity regulates cytokinesis in mammalian cells and points to the intriguing possibility that lysosome activity in close proximity to the intercellular bridge plays an essential role in this process.

RESULTS

CaBP7 localization in HeLa cells

In a previous study characterizing CaBP7 membrane targeting (Mc-Cue et al., 2011), we consistently observed a subpopulation of HeLa cells in which CaBP7 localized to vesicular structures in addition to the TGN. To identify these vesicles, we examined the localization of CaBP7 with defined subcellular markers (Figure 1). Initially, monomeric cherry fluorescent protein (mCh)–tagged CaBP7 was coexpressed with yellow fluorescent protein (YFP)–tagged markers. No colocalization was observed between mCh-CaBP7 and the early endosome marker Rab5a–enhanced YFP (EYFP; Figure 1Ai) or the autophagosome marker LC3β-EYFP (Figure 1Aii). Degrees of colocalization were observed between mCh-CaBP7 and the late endosome/lysosome markers LAMP1-EYFP and green fluorescent protein (GFP)–VAMP7 (Figure 1A, iii and iv). CaBP7 localization in this analysis was variable and ranged from entirely vesicular in some cells to a mixed Golgi/vesicular distribution in others (Figure 1, Ai,
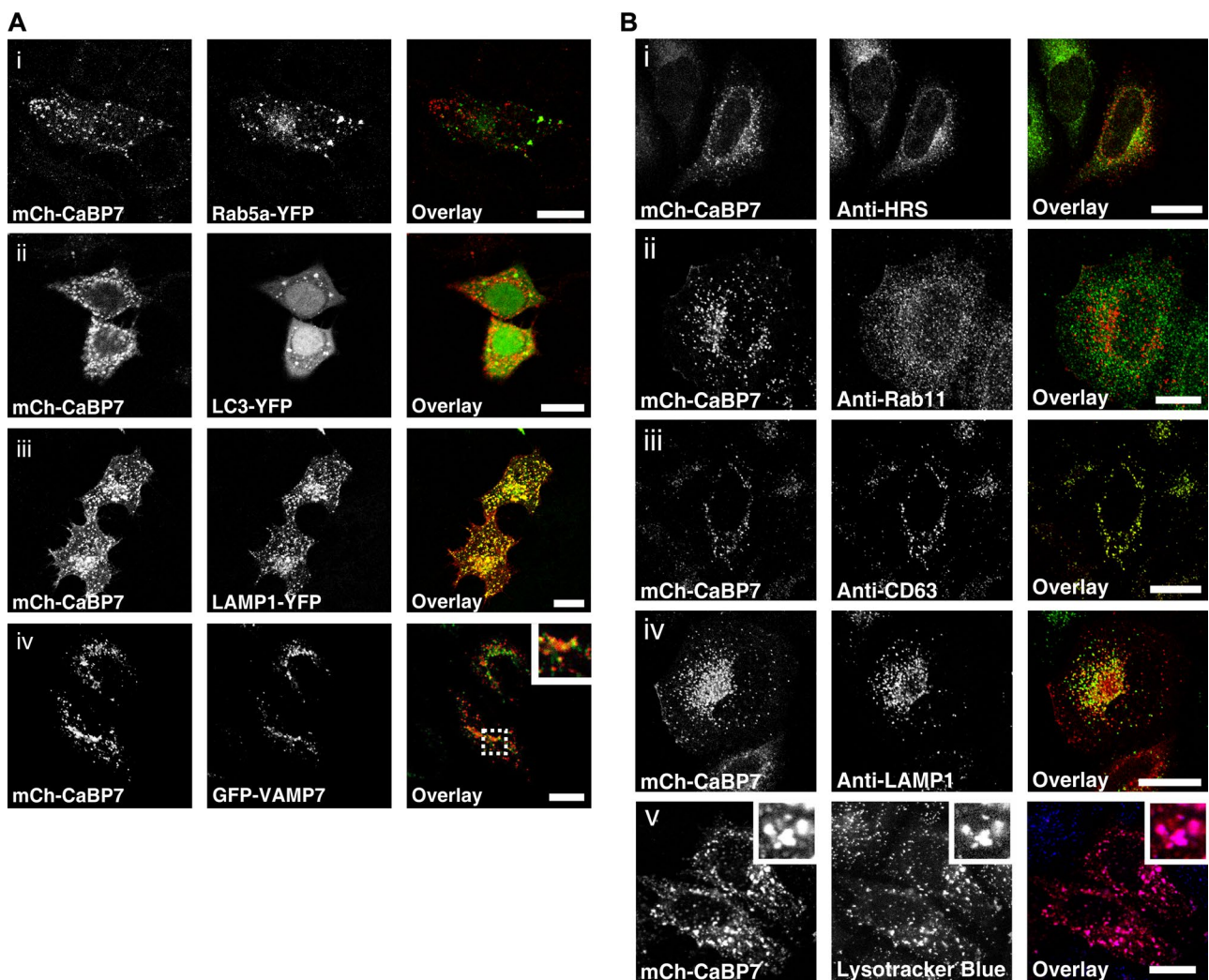

FIGURE 1: CaBP7 localization in HeLa cells. (A) Cells were transfected with mCh-CaBP7 along with EYFP-tagged Rab5a (i), LC3β (ii), LAMP1 (iii), or GFP-VAMP7 (iv). In overlays, mCh-CaBP7 is shown red and YFP/GFP markers in green. Inset in (iv) is an enlarged region of interest (ROI). (B) Cells transfected with mCh-CaBP7 were stained with the antibodies i) anti-HRS, ii) anti-Rab11, iii) anti-CD63, and iv) anti-LAMP1. mCh-CaBP7–transfected cells were also labeled with LysoTracker Blue (v, blue) before live-cell imaging (inset is an enlarged ROI). mCh-CaBP7 signal is red in all overlays, and antibody staining is green. Regions of colocalization are yellow for red/green channel overlap or pink for red/blue channel overlap. Scale bars, 10 μm.
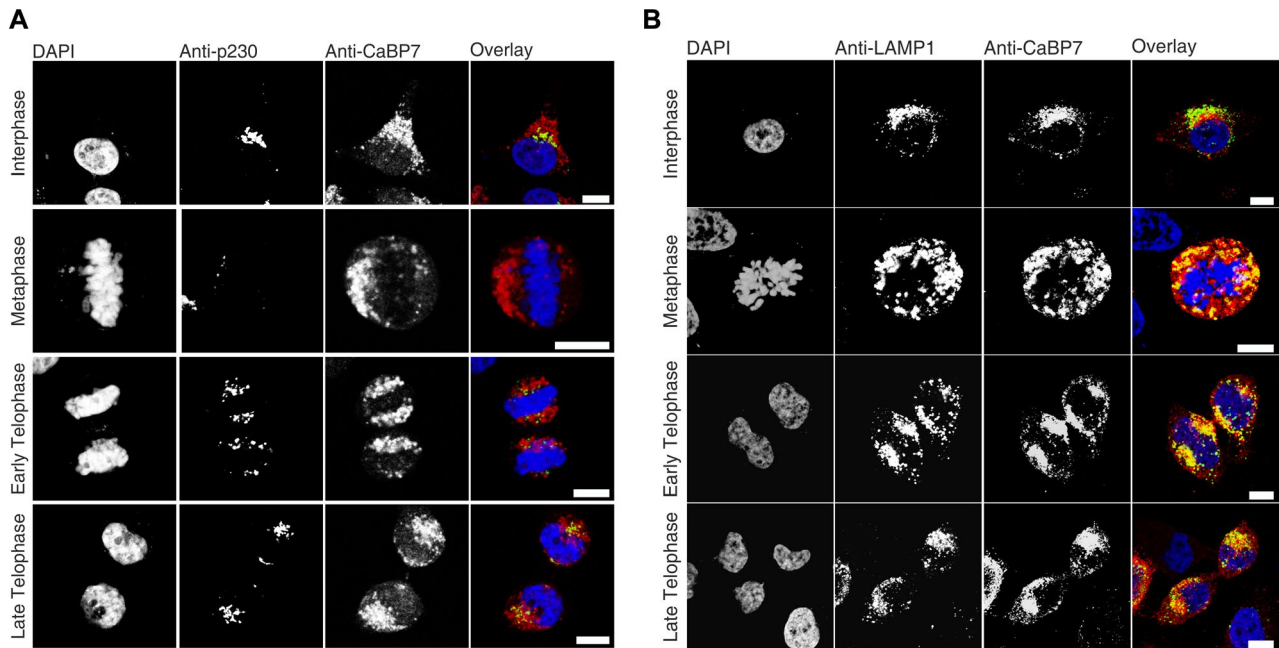
FIGURE 2: Distribution of endogenous CaBP7 with TGN and lysosomal markers during the cell cycle in fixed and live HeLa cells. (A) Cells were fixed and stained with DAPI (blue), anti-p230 (green), or anti-CaBP7 (red) antibodies. (B) Cells were fixed and stained with DAPI (blue), anti-LAMP1 (green). and anti-CaBP7 (red). Colocalization appears yellow in overlays. Scale bars, 10 μm.

vesicular, vs. Aiv, vesicular and Golgi). Similar data were obtained with endogenous markers (Figure 1B). mCh-CaBP7 did not localize with the multivesicular body protein HRS (Figure 1Bi) or the recycling endosome marker Rab11 (Figure 1Bii). Extensive colocalization of mCh-CaBP7 was observed with late endosome/lysosome markers LAMP1 and CD63 (Figure 1B, iii and iv). CaBP7 exhibited significant colocalization with LysoTracker Blue, which specifically labels endolysosomal compartments (Figure 1Bv). Collectively these data indicate that a significant proportion of CaBP7-positive vesicles are late endosomes/lysosomes.

CaBP7 exhibits cell cycle–dependent subcellular localization

To understand CaBP7's heterogeneous pattern of localization (see prior discussion), we examined its subcellular distribution with Golgi or lysosome markers during cell division. Because CaBP7 functions during cytokinesis (Neumann *et al.*, 2010), we reasoned that it might traffic in a cell cycle–dependent manner. Initially, the distribution of endogenous CaBP7 with the TGN marker p230 was assessed (Figure 2A). At interphase, there was colocalization of CaBP7 with p230 in a perinuclear region consistent with the TGN. At metaphase, p230 immunoreactivity was lost due to Golgi fragmentation; however, CaBP7 remained associated with vesicles. By early telophase, the Golgi apparatus had begun to reform, and CaBP7 partially colocalized with p230. At late telophase, the Golgi had fully reformed, and CaBP7/p230 partially colocalized to a level comparable to that observed during interphase (Figure 2A and Supplemental Table S1). Cell cycle–dependent localization of CaBP7 with the lysosomal marker LAMP1 was also tested (Figure 2B). At interphase, there was partial colocalization of these proteins (Supplemental Table S1). Colocalization increased at metaphase (explaining CaBP7 localization to vesicles in the absence of the Golgi). Colocalization increased further during early telophase and began to decline at late telophase (Supplemental Table S1). These observations were mirrored in live-cell imaging experiments monitoring mitotic progression in

HeLa cells transfected with CaBP7 and LAMP1 (Figure 3 and Supplemental Movie S1). Consistent with these data, PI4KIIIβ exhibited a similar localization profile during mitosis and cytokinesis (Figure 4). PI4KIIIβ concentrated in a perinuclear patch at interphase (the TGN). There was partial colocalization with LAMP1 in interphase cells, and during metaphase and telophase both proteins remained partially colocalized, consistent with a pool of PI4KIIIβ residing on lysosomes during mitosis. The derived Pearson's coefficients further highlight that of all markers assessed, CaBP7 colocalized to the greatest extent with the lysosomal marker LAMP1.

CaBP7 reduces PI4P levels and clusters lysosomes

Knowing that CaBP7 and PI4KIIIβ target to lysosomes, we examined whether CaBP7 could modulate PI4P levels in cells. Cells were transfected with mCh-CaBP7 and PI4P levels assessed with a PI4P-specific antibody (Figure 5A). On average, there was 58% reduction in PI4P-positive vesicle number in the presence of mCh-CaBP7 compared with controls (average 20.9 ± 1.6 PI4P particles/cell for mCh-CaBP7–transfected cells vs. average 49.9 ± 3.4 PI4P particles/cell for untransfected cells; Figure 5C). Because PI4P is a major precursor of phosphatidylinositol 4,5-bisphosphate (PIP_2) production, a prominent inositol lipid–signaling species with described functions during cytokinesis (Brill *et al.*, 2011; Echard, 2012), we next addressed whether CaBP7 might indirectly modulate levels of this lipid as a consequence of reducing PI4P production. Cells were transfected with mCh-CaBP7, and PIP_2 levels were assessed with a PIP_2-specific antibody (Figure 5B). Although we observed a small reduction in cellular PIP_2, this was not statistically significant compared with PIP_2 levels observed in untransfected control cells from the same experiment (Figure 5C). We also attempted to confirm the influence of CaBP7 overexpression on cellular PI4P levels by dot blot analysis using a PIP-Strip–based method (Supplemental Figure S1). No discernible difference in total cellular PI4P between control and CaBP7-transfected cells was observable using this approach. This is likely
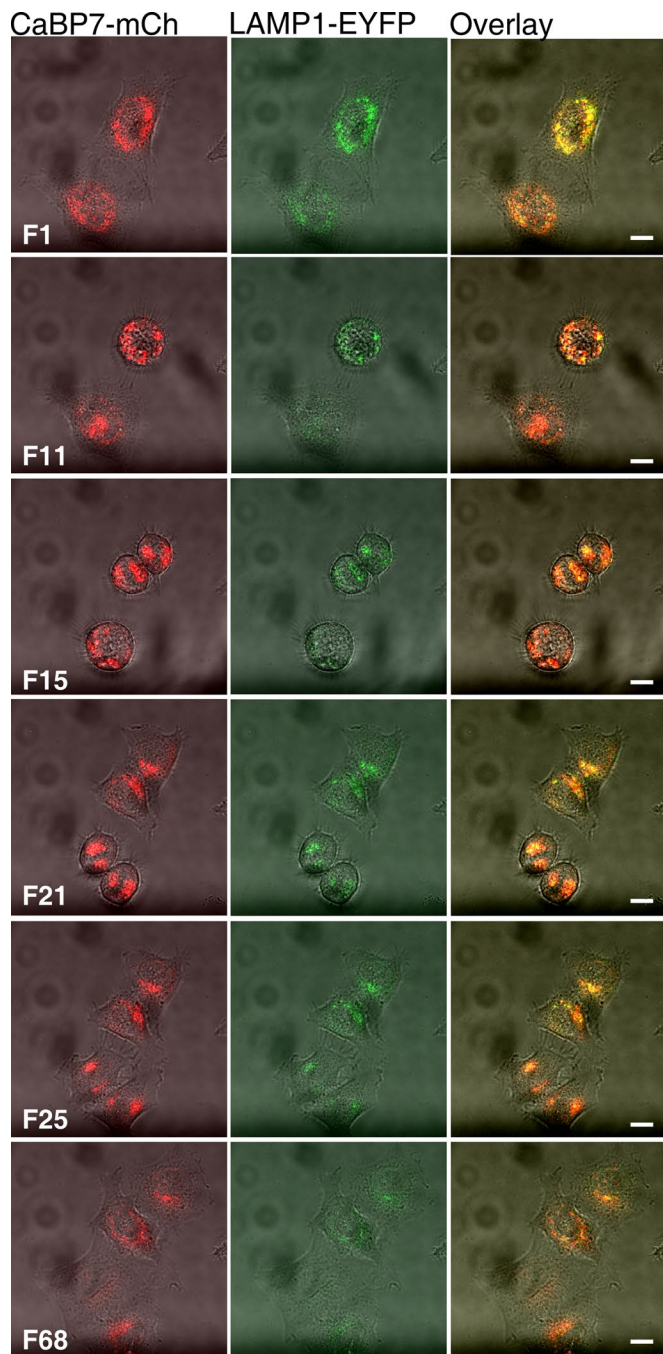
CaBP7-mCh   LAMP1-EYFP   Overlay

FIGURE 3: Live-cell imaging of cells transfected with CaBP7 and LAMP1 during mitosis. Cells were transfected with CaBP7-mCh (red) and LAMP1-EYFP (green) and imaged once every 11.67 min by confocal microscopy as described in *Materials and Methods*. Images are shown starting at frame 1 (F1), initiation of mitosis (prophase), through to frame 68, completion of cytokinesis. All images are additionally overlaid with the transmitted light channel to permit an assessment of cell morphology. Scale bars, 10 μm.

due to a combination of 1) limited transfection efficiency, 2) heterogeneity of CaBP7 expression in cells that were transfected, and 3 the CaBP7-regulated pool of PI4P representing a subpopulation of total cellular PI4P.

Inhibition of PI4KIIIβ to deplete PI4P results in clustering of lysosomes (Sridhar *et al.*, 2013). Consistent with this expression of

CaBP7, Ca^{2+}-deficient EF-hand mutants of CaBP7 and a kinase-dead PI4KIIIβ mutant can induce lysosome clustering, suggesting an effect on lysosomal PI4P (Supplemental Figure S2 and Supplemental Table S2). This was specific to lysosomes, since organelles earlier in the endolysosomal pathway were unaffected (Supplemental Figure S3).

CaBP7 and PI4P function during mitotic cell division (Liu *et al.*, 2008; Neumann *et al.*, 2010; Brill *et al.*, 2011; Echard, 2012). Because CaBP7 lowered PI4P levels and induced lysosome clustering, we examined potential connections between CaBP7, lysosomes, and mitosis. We first examined the distribution of CaBP7 during mitosis (Figure 6A). At interphase, CaBP7, as expected, localized to vesicles and a perinuclear region, consistent with the TGN. From metaphase through to completion of anaphase, CaBP7-positive structures aggregated and moved toward the cell periphery. At telophase, these vesicles redistributed from the periphery to flank the intercellular bridge. These data are consistent with a previous study in which lysosomal clustering during cytokinesis was observed (Matteoni and Kreis, 1987). Colocalization of CD63-positive endolysosomal compartments with CaBP7-positive vesicles was observed during all stages of mitosis (Figure 6B), suggesting that the majority of CaBP7 becomes lysosome associated during this process.

PI4KIIIβ activity influences normal completion of cytokinesis

Knowing that CaBP7-positive lysosomes exhibit an organized redistribution during cytokinesis and that CaBP7 controls PI4P levels in cells prompted us to examine the requirement for PI4KIIIβ activity during mitosis in HeLa cells (Supplemental Table S3 and Figure 7A). A previous study uncovered a role for CaBP7 during cytokinesis (Neumann *et al.*, 2010), and we used the same analysis to examine the role of PI4KIIIβ and its effectors during HeLa cell cytokinesis. First, we confirmed that CaBP7 depletion causes cytokinesis failure. CaBP7 knockdown and control transfected cells were imaged, and those harboring more than one nucleus were scored as abnormal (Figure 7A). Expression of scrambled short hairpin RNA interference (shRNAi) generated an 8.4% abnormal nuclei frequency (ANF), which increased to 22.9% on CaBP7 knockdown (Figure 7B). This 2.7-fold difference in ANF is consistent with the previous study (Neumann *et al.*, 2010). Of importance, the cytokinesis defect generated by CaBP7 protein depletion could be rescued by coexpression of a shRNAi-resistant version of the protein (Supplemental Table S3 and Figure 7B).

If CaBP7 depletion affected cytokinesis through loss of PI4KIIIβ inhibition, then overexpression of wild-type PI4KIIIβ or its activators (NCS-1 and ARF1) should elicit the same phenotype. To test this hypothesis, we examined how overexpression of PI4KIIIβ and its effectors influenced cytokinesis (Figure 7C). EYFP control protein elicited an 8.2% ANF, similar to that observed with control shRNAi expression (Supplemental Table S3 and Figure 7C). Overexpression of wild-type PI4KIIIβ and its activators NCS-1 and ARF1 (all predicted to increase PI4P production by PI4KIIIβ) generated ANFs of 17.9, 19.6, and 13.5%, respectively (Figure 7C and Supplemental Table S2). Overexpression of PI4KIIIβ^{D656A} or CaBP7, both of which should antagonize endogenous PI4KIIIβ, generated ANFs similar to those observed with control EYFP expression (7.8 and 6.8% ANF; respectively; Supplemental Table S3 and Figure 7C). These data are consistent with the hypothesis that excessive activation of PI4KIIIβ impairs cytokinesis in mammalian cells.

Depletion of CaBP7 induces loss of lysosomal clustering at cytokinesis

To understand how CaBP7 loss of function elicits cytokinesis failure, we examined lysosome distribution during mitosis in
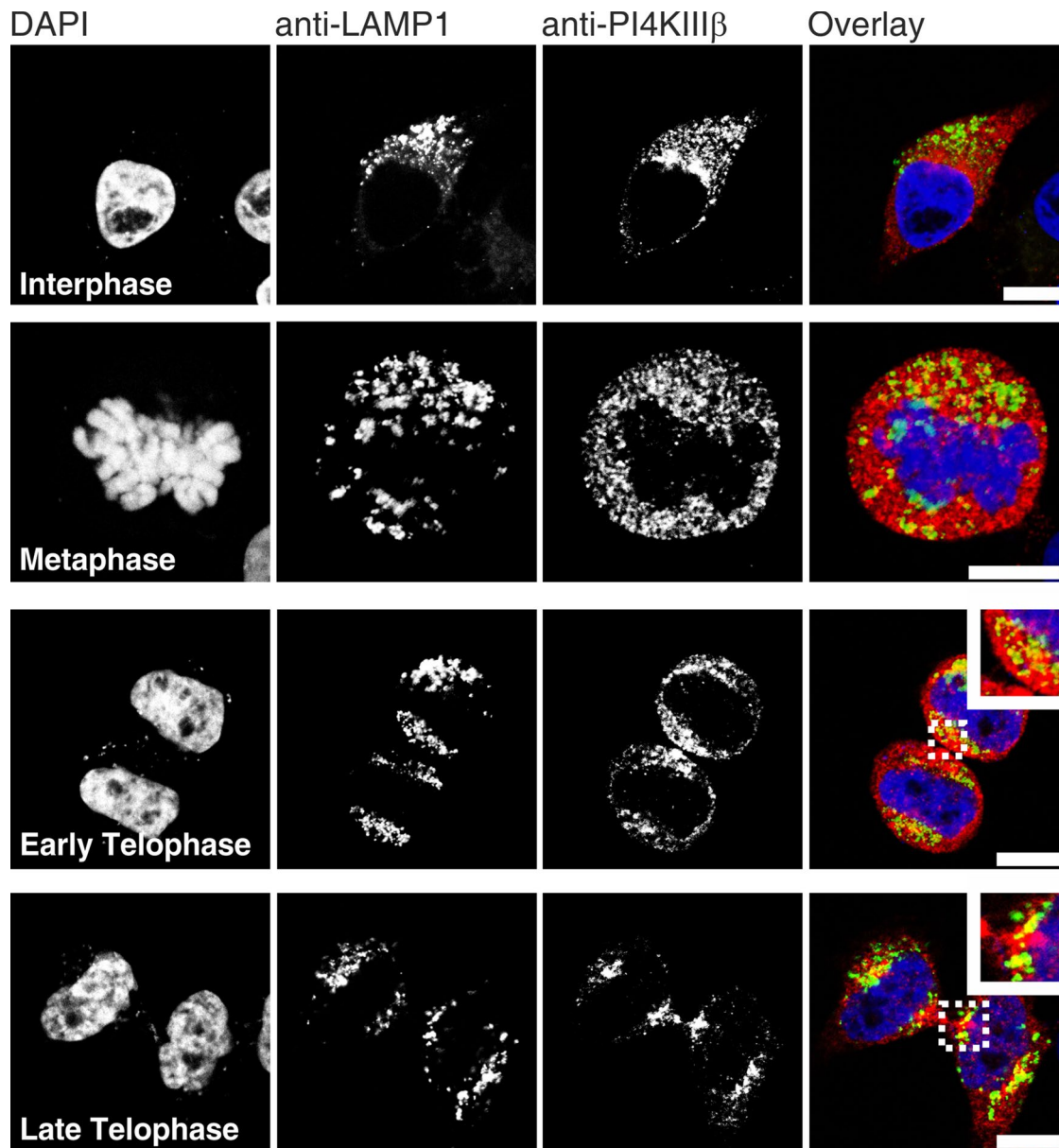
FIGURE 4: Distribution of PI4KIIIβ with LAMP1 during mitosis. Cells were stained with anti-PI4KIIIβ antibody (red), anti-LAMP1 (green), and DAPI (blue). Inset regions in telophase overlay images are enlargements of the ROI highlighted (white dotted square). Cells are shown at stages of the cell cycle. Colocalization between LAMP1 and PI4KIIIβ appears yellow in overlay images. Scale bars, 10 µm.

CaBP7-knockdown cells versus controls (Figure 8, A–C). Lysosomes cluster near the intercellular bridge at cytokinesis (Figures 2B and 6B; Matteoni and Kreis, 1987). In shRNAi control cells, clustering was observed (Figure 8A). CaBP7 shRNAi–expressing cells exhibited a marked loss of clustering at the intercellular bridge during cytokinesis (Figure 8A). This was quantified by calculating LAMP1 fluorescence intensity in the intercellular bridge region (Figure 8C). Consistent data were acquired from live-cell experiments in which LysoTracker Red was monitored during mitosis and cytokinesis in cells depleted of CaBP7 and compared with untransfected cells on the same dish (Figure 9 and Supplemental Movies S2 and S3). Loss of LAMP1 fluorescence at the intercellular bridge was not due to CaBP7 shRNAi expression causing a reduction in lysosome numbers, as total cellular LAMP1 fluorescence was similar in both CaBP7 shRNAi and scrambled control cells (Supplemental

Figure S4). Finally, we investigated whether loss of lysosomal clustering on CaBP7 depletion was specific for these organelles by examining the distribution of the TGN at cytokinesis (Figure 8, B and C). No difference in p230 distribution in cells at cytokinesis was observed between scrambled and CaBP7 knockdown conditions (Figure 8, B and C). Because we previously demonstrated that CaBP7 overexpression was able to deplete cellular PI4P levels in interphase cells (Figure 5A), we tested whether this was also observable in mitotic cells (Figure 8D). Indeed, overexpression of CaBP7 qualitatively reduced PI4P staining compared with that observed in untransfected control cells. These data suggest that CaBP7 can modulate PI4P levels during cytokinesis in HeLa cells.

Closer analysis of live-cell imaging data showed that in control, untransfected cells at cytokinesis, the intercellular bridge had an
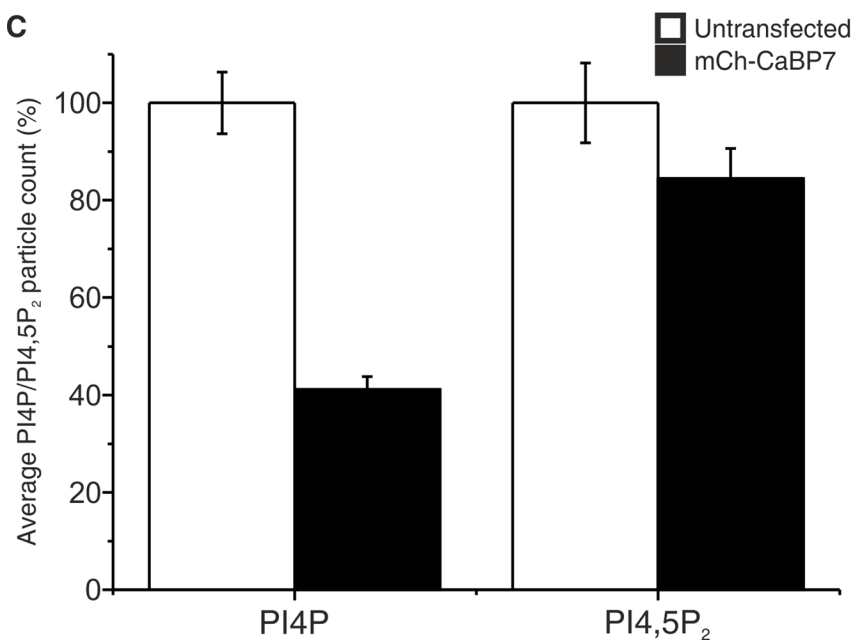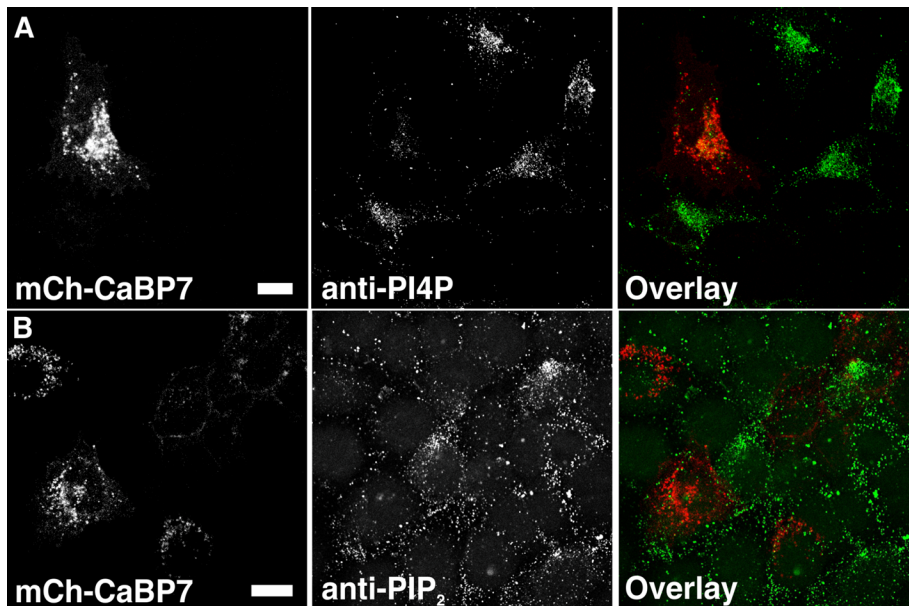
FIGURE 5: CaBP7 reduces PI4P but not PI4,5P$_2$ levels in HeLa cells. Cells were transfected with mCh-CaBP7 (red; A, B) and stained with anti-PI4P antibody (green; A) or anti PI4,5P$_2$ antibody (green; B). The number of PI4P- and PI4,5P$_2$-positive vesicles per cell was determined for mCh-CaBP7–transfected vs. untransfected cells on the same coverslip. Scale bars, 10 μm. (C) Quantification of data from A and B. All data are plotted as mean ± SEM. Untransfected control cells ($n = 51$) and mCh-CaBP7 transfected cells ($n = 39$) were analyzed from two independent experiments for PI4P samples. Untransfected control cells ($n = 36$) and mCh-CaBP7–transfected cells ($n = 36$) were analyzed from two independent experiments for PI4,5P$_2$ samples.

average lifetime of 25.2 ± 2.4 min (Supplemental Movie S4 and Supplemental Figure S5). In contrast, cells depleted of CaBP7 exhibited a 3.4-fold increase in the lifetime of the intercellular bridge (86.7 ± 9.0 min; Supplemental Movie S5 and Supplemental Figure S5). This could indicate that loss of CaBP7 induces a problem with bridge stability/assembly or abscission (Barr and Gruneberg, 2007; Mierzwa and Gerlich, 2014).

DISCUSSION

This study was initiated by the novel observation that in addition to association with the TGN, CaBP7 was present on various uniformly distributed cytoplasmic vesicles in some but not all cells (McCue et al., 2009). On closer inspection, we were able to identify the CaBP7-positive vesicles not as secretory cargo carriers but, somewhat unexpectedly, as late endosomes/lysosomes. CaBP7 has been implicated as a factor required for normal completion of cytokinesis in mammalian cells (Neumann et al., 2010). This led us to examine whether CaBP7 might exhibit cell cycle–dependent localization, which might also explain the heterogeneity in CaBP7 distribution between cells within a population. Our data indicate that during interphase, CaBP7 is Golgi and lysosome resident, but that as cells enter mitosis, the protein relocates to become more lysosomal. This shift in CaBP7 distribution begins to reverse during cytokinesis, consistent with a proportion of CaBP7 returning to the TGN at reestablishment of interphase. A recent study in mammalian cells reported that a biochemically distinct pool of PI4KIIIβ is lysosomally associated and its activity there is essential for lysosomal content sorting (Sridhar et al., 2013). Based on our cell cycle–dependent localization data, a candidate PI4KIIIβ interaction partner localized to lysosomes was CaBP7. PI4KIIIβ is the only documented target for CaBP7, and we therefore reasoned that lysosomal CaBP7 might regulate the PI4KIIIβ pool resident at these organelles. Consistent with this hypothesis, we demonstrated that overexpression of CaBP7 significantly reduced cellular PI4P levels in both interphase and mitotic cells. These observations were corroborated and linked specifically to lysosomal PI4P by using a simple lysosomal clustering assay developed by Sridhar et al. (2013). We were able to show that CaBP7 overexpression elicited a similar lysosomal clustering phenotype observed when endogenous PI4KIIIβ activity is reduced through RNAi-mediated protein depletion (Sridhar et al., 2013) or overexpression of the dominant-negative, kinase-dead version of the enzyme (Sridhar et al., 2013; Supplemental Figure S1). Collectively these data are consistent with a model in which PI4KIIIβ activity, regulated at least in part by CaBP7, is able to control lysosomal positioning, a property that is misregulated through inhibition of the enzyme and depletion of a lysosomal pool of PI4P.

PI4KIIIβ has also been implicated as an important factor regulating mitosis and cytokinesis in a number of model organisms; however, the importance of PI4KIIIβ activity during the process of cell division in mammalian cell systems has yet to be assessed. We sought to determine whether CaBP7 influenced cytokinesis via PI4KIIIβ, in light
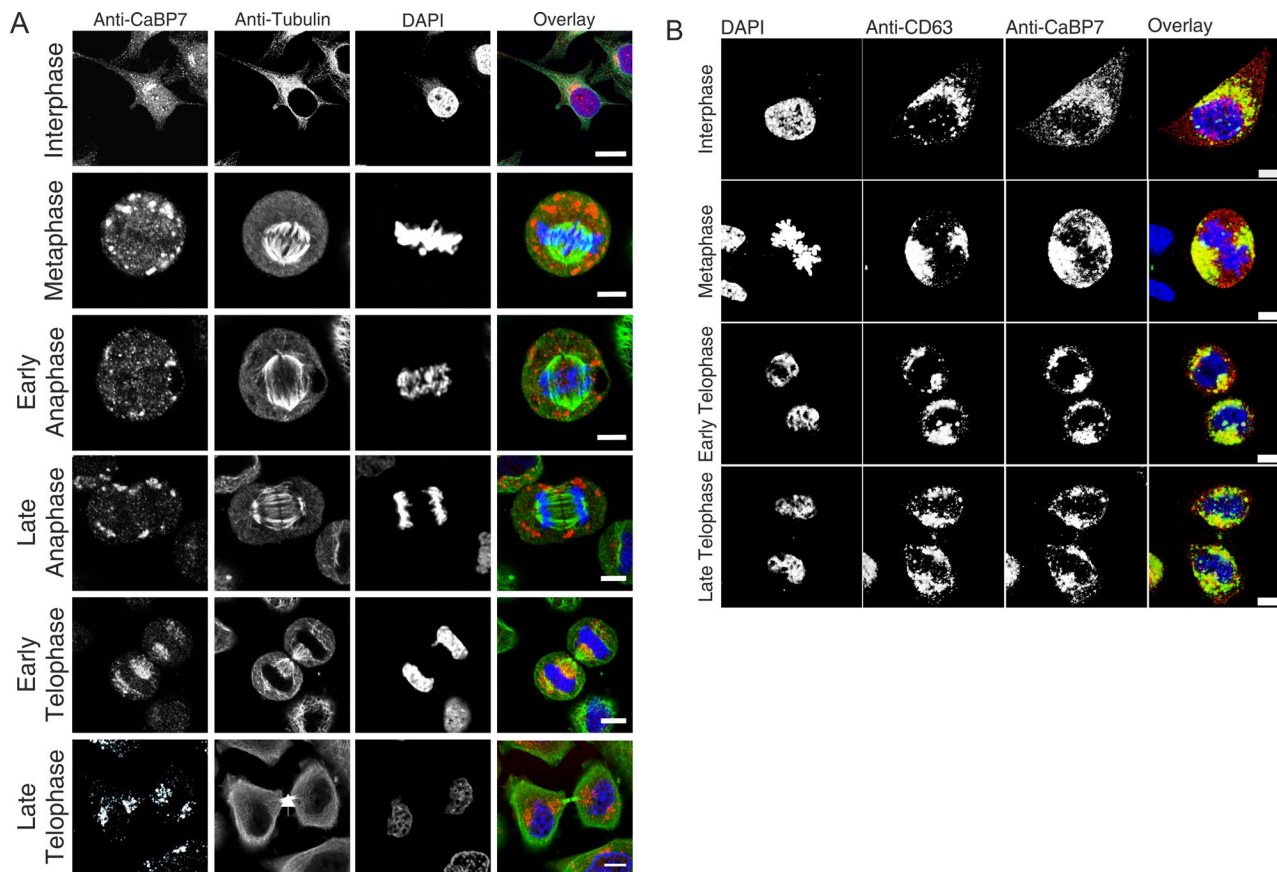
FIGURE 6: Distribution of CaBP7-positive vesicles during HeLa cell mitosis. (A) Cells were stained with DAPI (blue), anti-CaBP7 (red), and anti–α-tubulin (green). CaBP7 distribution was monitored at interphase and at defined points during mitotic cell division (metaphase through to late telophase—cytokinesis, arrowhead in anti-tubulin image highlights the intercellular bridge). CaBP7 and tubulin colocalization is yellow in overlay images. (B) Cells stained with DAPI (blue) were costained with anti-CaBP7 (red) and anti-CD63 (green) antibodies. CaBP7/CD63 distribution was characterized at interphase and in cells at metaphase, early telophase, and late telophase. CaBP7 and CD63 colocalization is yellow in overlay images. Scale bars, 10 μm.

of experimental evidence that disruption of PI4P levels is detrimental to this process in model organisms. We addressed potential functional consequences of PI4KIIIβ activity and alterations in the pool of PI4P controlled by this kinase during HeLa cell mitosis and provided new evidence suggesting that it is an important factor in mammalian cell division. We were able to demonstrate that factors elevating PI4P production by PI4KIIIβ, including shRNAi-mediated depletion of endogenous CaBP7 protein or overexpression of PI4KIIIβ or its activators, all disrupt cytokinesis and generate binucleate or multinucleate cells likely through stabilization of the intercellular bridge, incomplete bridge assembly, or defective abscission. The precise defect requires further examination of bridge-specific structures and whether their appearance is disrupted by loss of CaBP7 activity. Conversely, factors inhibiting PI4P production, including overexpression of exogenous CaBP7, have no effect on normal progression through mitosis and successful cytokinesis. Our findings are in contrast to those from *Drosophila*, in which PI4KIIIβ Fwd has been reported to be required for cytokinesis (Polevoy *et al.*, 2009). Note, however, that this applied only to spermatocytes and not somatic cells and that part of the requirement for Fwd was in a nonenzymatic capacity.

We showed that alterations in PI4KIIIβ activity can affect lysosomal dynamics and that loss of CaBP7 function prevents organized lysosome clustering at the intercellular bridge during cytokinesis. It has been known for >25 yr that lysosomes cluster in a cell cycle–specific manner (Matteoni and Kreis, 1987), but why has remained a mystery. Lysosomes could conceivably mediate a degradative role to remove cytoskeletal components before membrane fission can proceed or provide a membrane reservoir required for completion of abscission, as shown for endosomes (Boucrot and Kirchhausen, 2007). Lysosomes do exhibit membrane donor behavior during plasma membrane repair (McNeil and Kirchhausen, 2005; Luzio *et al.*, 2007a). Lysosomes have also been recognized to mediate another key cellular role by acting as focal Ca^{2+}-signaling platforms (Galione and Chuang, 2012; McCue *et al.*, 2013). The role of Ca^{2+} during mitosis has been established in model cell systems (Miller *et al.*, 1993; Whitaker, 2006); however, the significance of intracellular Ca^{2+}-signals during mammalian cell mitosis remains unclear. This report characterizes the novel finding that a specific Ca^{2+}-binding protein directly affects normal cytokinesis through regulation of phosphoinositide signaling. Our observations raise a number of interesting possibilities, and further work will be required to ascertain whether one or a combination of lysosomal activities (Ca^{2+} handling, recycling of cellular debris, membrane donation) contribute to cytokinesis in mammalian cells.
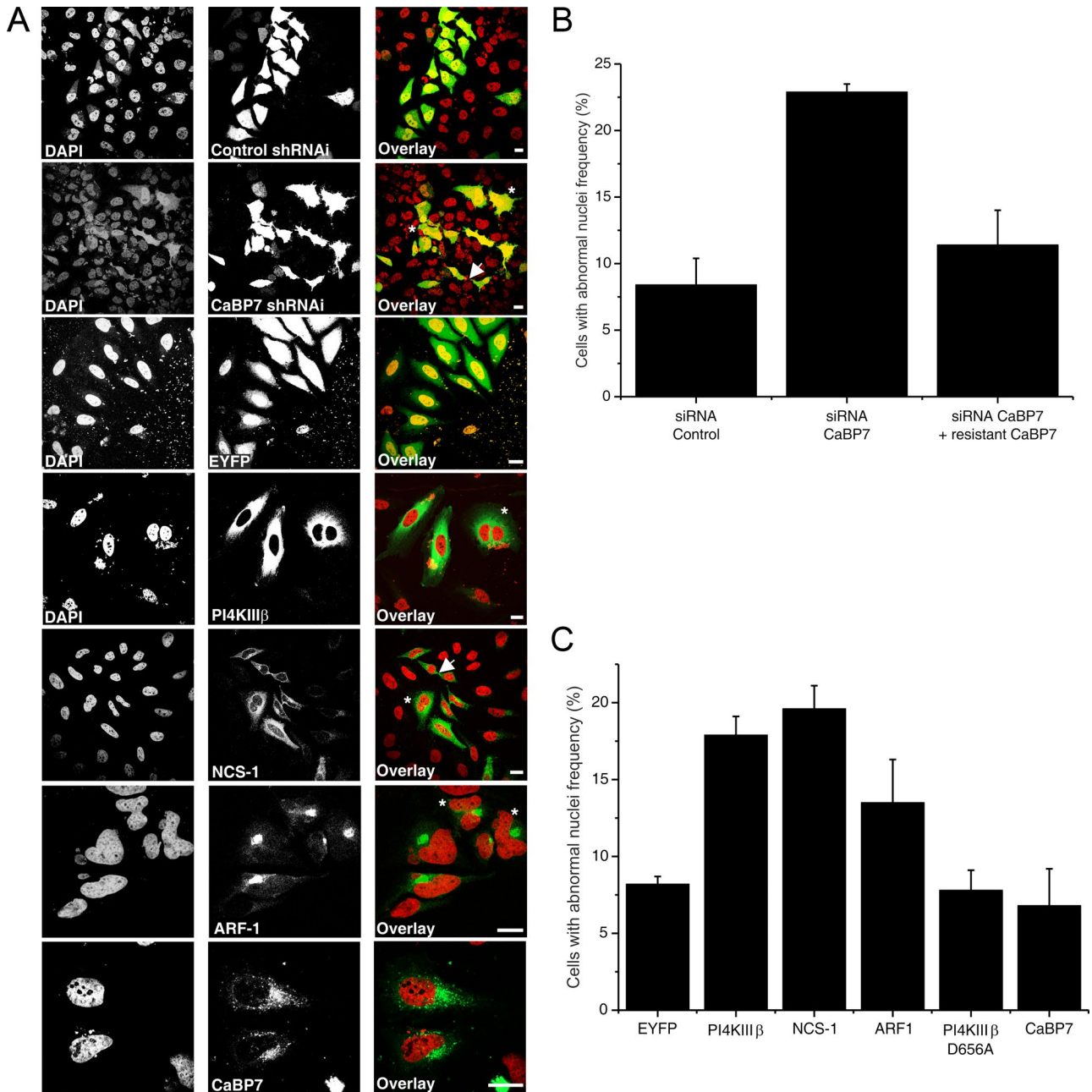
FIGURE 7: PI4KIIIβ activity influences cytokinesis. (A) Cells transfected with constructs able to modulate PI4KIIIβ activity were stained with DAPI (red). Samples were scored for the number of multinucleate cells and cells at cytokinesis connected by an intercellular bridge. Cells were transfected with CaBP7 or scrambled control shRNAi plasmids. Silencing plasmids expressed GFP as a transfection marker (green). Overexpression of PI4KIIIβ, NCS-1, ARF1, PI4KIIIβ[D656A], and CaBP7 was also tested in this assay with EYFP as a control (all overexpressed constructs are green in overlays). Multinucleate cells are highlighted with an asterisk and cells undergoing cytokinesis with an arrowhead. Scale bars, 10 μm. (B) Quantification of shRNAi data from A. All data are plotted as mean ± SEM. Students unpaired t test analysis was performed for silencing data sets where CaBP7 knockdown and rescue were compared with scrambled control ($p < 0.0001$ for both conditions). (C) Quantification of overexpression conditions from A. Students unpaired t test analysis comparing each data set to the EYFP control condition generated $p < 0.0001$ in all instances, with the exception of ARF1, for which $p = 0.0127$. Statistical data are summarized in Supplemental Table S3.

MATERIALS AND METHODS
Plasmid constructs
mCherry-CaBP7, CaBP7-mCherry (mCh-CaBP7/CaBP7-mCh), and EYFP-CaBP7 were generated as previously described (McCue et al., 2009). mCh-CaBP7 EFx2 (E56Q, E93Q) double mutation and EF 1 (E56Q) and EF2 (E93Q) single mutations were all made by QuikChange site-directed mutagenesis according to the manufacturer's protocol (Agilent, Santa Clara, CA). For mCh-CaBP7 EF1 and mCh-CaBP7 EF2 mutations, mCh-CaBP7 was used as template with sense primer 5′-TTCATCCAAGCA-GCAGCTGGGCACAGCCATG-3′ and antisense primer 5′-CATG-GCTGTGCCCAGCTGCTGCTTGGAGATGAA-3′ and sense primer
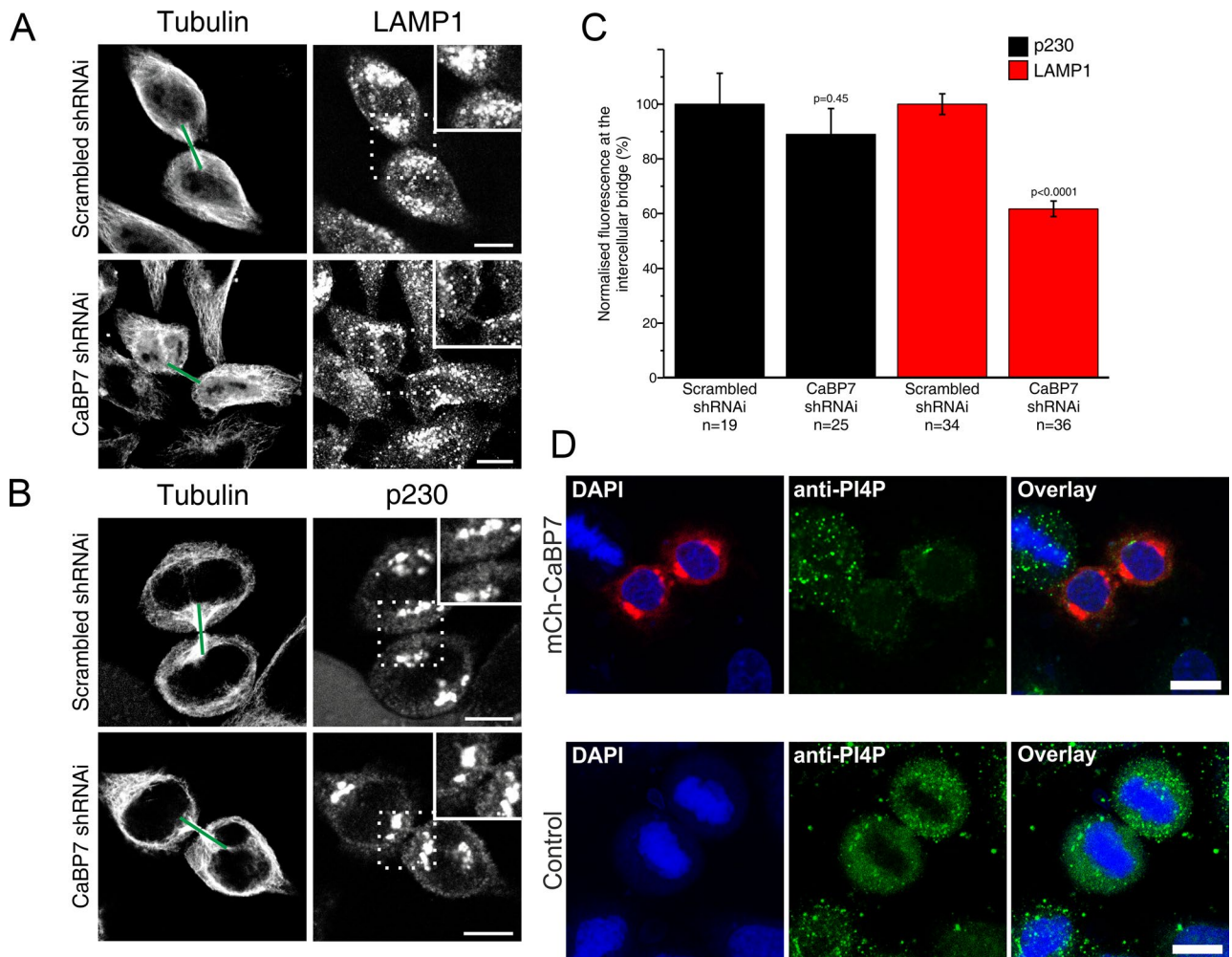
FIGURE 8: Analysis of CaBP7 depletion on lysosome and Golgi localization during cytokinesis. (A) Cells transfected with control or CaBP7 shRNAi plasmids were stained with LAMP1 and α-tubulin antibodies. Cells at cytokinesis were imaged and LAMP1 fluorescence intensity in the region spanning the intercellular bridge (green lines in tubulin images) analyzed as described in *Materials and Methods*. (B) The same analysis from A was performed on cells stained for α-tubulin and the TGN marker p230. Dashed boxes highlight the enlarged region in the insets (top right corner of p230/LAMP1 images). Scale bars, 10 μm. (C) Quantification of data from A and B. All data are plotted as mean ± SEM (*n* = 3 independent experiments) and analyzed for statistical significance (scrambled control vs. CaBP7 shRNAi for both LAMP1 and p230 samples) using the Student's unpaired *t* test. Total number of cells (*n*) analyzed across all three experiments is shown. (D) HeLa cells transfected with mCherry-CaBP7 (mCh-CaBP7, red) were costained with DAPI (blue) and anti-PI4P (green). Representative images for CaBP7- expressing and untransfected control cells from the same coverslips are shown for cells at early telophase. Scale bars, 10 μm.

5′-CAAGTGGACTTTGAGCAGTTTGTGACCCTTCTG-3′ and anti-sense primer 5′-CAGAAGGGTCACAAACTGCTCAAAGTCCAC-TTG- 3′, respectively. For mCh-CaBP7 EFx2 double mutation, mCh-CaBP7 EF1 was used as template with the sense primer and anti-sense primer used for EF2 mutation generation. CaBP4-mCh, ARF1-YFP, NCS1-YFP, and NCS-1-mCherry were described previously (Haynes *et al.*, 2005; McCue *et al.*, 2009; Handley *et al.*, 2010). HA-PI4KIIIβ and the kinase-dead D656A mutant were as previously described (Godi *et al.*, 1999). Rab5a-EYFP, LAMP1-EYFP, and LC3β-EYFP were as previously described (McCue *et al.*, 2013). GFP-VAMP7 was a kind gift from T. Galli, Institut National de la Santé et de la Recherche Médicale (Paris, France). CaBP7 shRNAi and scrambled control shRNAi plasmids were from OriGene (Cambridge, United Kingdom). The sequence for scrambled shRNAi was 5′-GCACTACCAGAGCTAACTCAGATAGTACT-3′. The CaBP7-specific shRNAi sequence was 5′-GACATGGATGGTGATG-

GTCAAGTGGACTT-3′. The plasmids encode a 29-mer shRNAi under control of the human U6 promoter and a separate GFP reporter under the control of the CMV promoter for verification of transfection. shRNAi-resistant mCh-CaBP7 was generated by introduction of three silent point mutations using site-directed mutagenesis with sense primer 5′-GACATAGAGAACAT**a**AT**t**ATGAC**a**GAGGAG-GAG-3′ and antisense primer 5′-CTCCTCCTC**t**GTCAT**a**AT**t**ATGTT-CTCTATGTC-3′. Point mutations are highlighted in boldface. All new plasmid constructs were verified by automated sequencing (Sequencing Service, University of Dundee, Dundee, United Kingdom).

Cell culture and plasmid transfections
HeLa cells were cultured in DMEM supplemented with 10% (vol/vol) fetal bovine serum, 1% (vol/vol) penicillin/streptomycin, and 1% (vol/vol) nonessential amino acids. All cells were maintained in a humidified atmosphere of 95% air/5% CO_2 at 37°C. Cells were
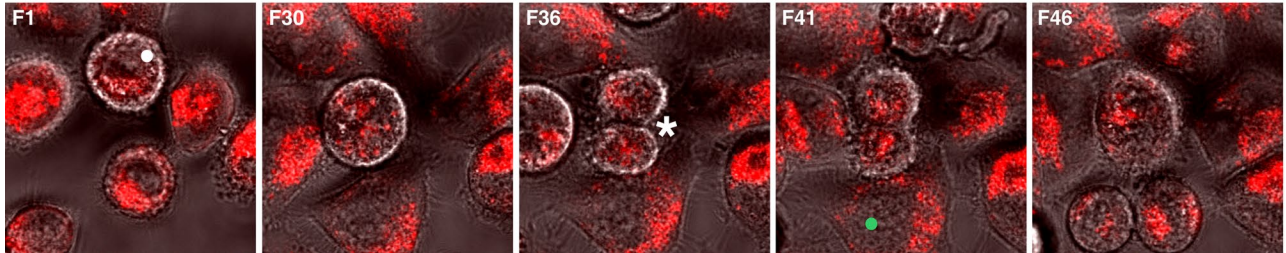
Non-transfected
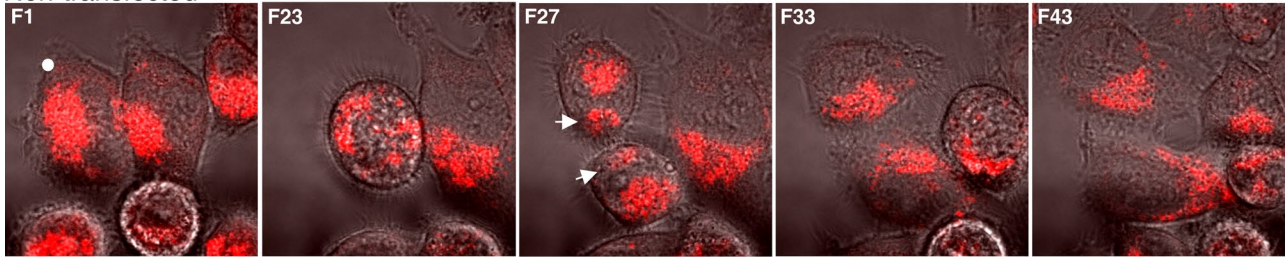
CaBP7 shRNAi

FIGURE 9: CaBP7 silencing prevents lysosome clustering during cytokinesis in live HeLa cells. HeLa cells were transfected with CaBP7-specific shRNAi plasmid and loaded with LysoTracker Red. The silencing plasmid additionally expressed GFP as a marker for transfection (not shown). A control untransfected cell and one that was GFP positive (CaBP7 shRNAi transfected) that subsequently underwent mitosis are highlighted with a white circle in frame 1 images. Lysosome clustering at cytokinesis is highlighted (arrowheads, F27) in control cells. Corresponding clustering was not observed at the same stage of mitosis in CaBP7 depleted cells (*, F36). In addition, an untransfected cell in the CaBP7 silencing sample positioned directly beneath the CaBP7-depleted cell (green circle, F41) underwent normal mitosis and exhibited normal clustering of LysoTracker Red–positive vesicles. The CaBP7-depleted cell failed to complete cytokinesis successfully and became binucleate.

plated onto sterile, 13-mm-round coverslips at a density of 0.25 × 10^6 cells/well for fixation or directly onto 24-well tissue culture trays for Western blotting purposes. After 24 h, cells were transiently transfected with the indicated expression vectors using GeneJuice transfection reagent (Merck Millipore, Darmstadt, Germany) according to the manufacturer's protocol. For single and double transfections, 1 μg of each plasmid was used.

Immunofluorescence and imaging

At 24 h posttransfection (72 h for knockdown studies), cells on coverslips were washed with phosphate-buffered saline (PBS; 137 mM NaCl, 2.7 mM KCl, 10 mM Na_2PO_4, 2 mM NaH_2PO_4, pH 7.4) and then fixed with 4% (vol/vol) formaldehyde in PBS for 6 min at room temperature. Coverslips were subsequently air dried and mounted onto microscope slides using Prolong antifade glycerol (with or without 4′,6-diamidino-2-phenylindole [DAPI] nuclear stain; Life Technologies, Paisley, UK). For immunofluorescence studies, cells were washed and fixed as described, followed by permeabilization with 0.2% (vol/vol) Triton-X-100 in PBS for 6 min at room temperature. Cells were washed extensively with PBS and twice with blocking solution (5% [wt/vol] bovine serum albumin [BSA] in PBS). Primary antibodies used were as follows: mouse monoclonal anti-hemagglutinin (1:500; Sigma, Poole, United Kingdom); Mouse monoclonal anti-LAMP1 (1:400; AbCam, Cambridge, United Kingdom); mouse monoclonal anti-PI4P (1:100; Echelon Biosciences, Salt Lake City, UT); mouse monoclonal anti-PI4,5P$_2$ (1:200; Echelon Biosciences); mouse monoclonal anti-CD63 fluorescein isothiocyanate (FITC) conjugate (1:200; AbCam); rabbit polyclonal anti-Rab11 (1:500; Life Technologies); rabbit polyclonal anti-CaBP7 (1:200; Santa Cruz Biotechnology, Dallas, TX); mouse polyclonal anti-p230 (1:200; BD Biosciences, Oxford, United Kingdom); mouse mono-

clonal anti–α-tubulin (1:500; AbCam); rabbit polyclonal anti–mannose-6-phosphate receptor (1:500; a kind gift from Paul Luzio, University of Cambridge, Cambridge, United Kingdom) and rabbit polyclonal anti-HRS (1:1000; a kind gift from Sylvie Urbé, University of Liverpool, Liverpool, United Kingdom). Primary antibodies were applied overnight at 4°C with gentle agitation. Cells were washed three times with 1 ml of PBS and twice with 1 ml of blocking solution and incubated with secondary goat anti-mouse immunoglobulin G (IgG) conjugated to Alexa Fluor 488 or 405 for 1 h at room temperature (with the exception of FITC-conjugated anti-CD63). Coverslips were washed three times with 1 ml of PBS and then air dried and mounted onto microscope slides using Prolong. For anti-PI4P staining, the staining protocol was modified as follows: Cells were fixed with 4% (vol/vol) formaldehyde/Tris-buffered saline (TBS; 50 mM Tris-HCl, pH 7.4, 150 mM NaCl) for 20 min at room temperature and washed subsequently three times with TBS. Permeabilization was achieved by incubating the cells with 0.5% (wt/vol) saponin in TBS at room temperature for 15 min. Cells were washed three times with TBS and then blocked with 10% (vol/vol) goat serum in TBS for 30 min at 37°C. Anti-PI4P antibody diluted in TBS was added to cells and incubated for 60 min at 37°C. Antibody was removed and cells washed three times with 1% (vol/vol) goat serum in TBS before secondary antibody incubation (30 min at 37°C). Secondary antibody was also diluted in TBS. Cells were rinsed thoroughly with distilled water, air dried, and mounted onto microscope slides with Prolong. Fixed cells were imaged using a Leica TCS-SP-MP confocal system (Leica Microsystems, Heidelberg, Germany) with pinhole set to 1 Airy unit and a 63× oil immersion objective with a numerical aperture of 1.3. Images were exported as TIFF files and compiled, processed, and analyzed with ImageJ and CorelDraw X6 applications.

Particle counting analysis

A representative untransfected control cell stained with anti-PI4P antibody was chosen and 25 randomly distributed PI4P positive particles selected. The diameters of these particles was determined using ImageJ, and the lower and upper limits of the range (8 and 15 pixels, respectively) was subsequently used to set a range (8–15 pixels) of particle diameters that would be detected by automated ImageJ counting. Particles having diameters smaller or larger than the limits of this range were therefore excluded from the analysis. For lysosomal clustering analysis, a minimum particle diameter of 10 pixels was used, with the maximum value set to infinity.

Fluorescence colocalization analysis with JACoP

The ImageJ plug-in JACoP (Bolte and Cordelieres, 2006) was used to derive Pearson's correlation coefficients for pairwise sets of image data. The Pearson's coefficient under these circumstances measures the strength of relationship between pixels at the same location in two images being compared. Perfect correlation (colocalization) generates a correlation coefficient, R, of 1. Briefly, each image was first subjected to background subtraction before analysis with JACoP. Costes' randomization was simultaneously applied for each pair of images analyzed to ensure the validity of the correlation data. For all image pairs analyzed, the randomized control Pearson's coefficient was 0 ± 0.003.

Analysis of lysosome/Golgi localization during cytokinesis

GFP-positive cells (a transfection marker present in CaBP7 shRNAi and scrambled shRNAi plasmids) at cytokinesis (determined through α-tubulin intercellular bridge staining) were analyzed with ImageJ software and the plot profile application. A straight line across the intercellular bridge extending to the edge of the nucleus of each daughter cell was drawn on p230/LAMP1-stained sample images and the fluorescence profile along this line analyzed. The area under the curve for these profiles was calculated, which represents the average fluorescence intensity of p230/LAMP1 in the regions of the cytoplasm and intercellular bridge directly beneath the line. Data from scrambled shRNAi samples were normalized to 100% (control) and CaBP7 shRNAi fluorescence intensity calculated as a percentage of this. Whole-cell fluorescence data were also analyzed from the same cells by tracing a region of interest around the plasma membrane of each cell and quantifying the average p230/LAMP1 fluorescence intensity over this area.

Lipid extraction and dot blot analysis

HeLa cells were plated onto 10-cm dishes and transfected with 5 μg of mCherry-N1 or 5 μg of mCherry-CaBP7. At 24 h posttransfection, cells ($\sim 2.2 \times 10^6$ cells/dish) were trypsinized, collected, and homogenized in 1 ml of chloroform/methanol 2:1 (vol/vol). After dispersion, the mixture was agitated at room temperature) on an orbital shaker (30 rpm) for 15 min. The homogenate was centrifuged at $2400 \times g$ for 3 min to recover the aqueous phase and the organic solvent washed with 200 μl of 0.9% (wt/vol) NaCl solution. After vortexing, the mixture was centrifuged at $380 \times g$ to again separate organic/aqueous phases. The upper phase was discarded and the interface surface rinsed twice with methanol/water 1:1 (vol/vol). The lower phase was subsequently centrifuged for 45 min at 43°C (medium drying rate) under vacuum to evaporate chloroform (SpeedVac SC210A). Lipid pellets were resuspended in 50 μl of chloroform/methanol 2:1 (vol/vol). From this sample, two further dilutions (twofold and fourfold) were prepared. A 1-μl sample of each was spotted onto a PIP-Strip (Echelon Biosciences) between the lipid standards and allowed to dry completely. Once dried, the filter was incubated

with blocking buffer (BB; 3% [wt/vol] BSA in 0.1% [vol/vol] Tween-20/PBS [PBS-T]) overnight at 4°C. The filter was then incubated with 0.5 μg/ml PI4P-Grip protein (Echelon Biosciences) in BB for 1 h at room temperature with gentle agitation. After three washes with PBS-T, the filter was incubated with anti–glutathione S-transferase antibody (rabbit polyclonal; Sigma) diluted 1:500 in BB for 1 h at room temperature with gentle agitation. The filter was subsequently washed three times with PBS-T and incubated with horseradish peroxidase–conjugated anti-rabbit IgG (Sigma) diluted 1:400 in BB for 1 h at room temperature with gentle agitation. Bound protein was visualized with enhanced chemiluminescence reagents.

REFERENCES

Baker DJ, Chen J, van Deursen JM (2005). The mitotic checkpoint in cancer and aging: what have mice taught us? Curr Opin Cell Biol 17, 583–589.

Balla T (2013). Phosphoinositides: tiny lipids with giant impact on cell regulation. Physiol Rev 93, 1019–1137.

Barr FA, Gruneberg U (2007). Cytokinesis: placing and making the final cut. Cell 131, 847–860.

Bolte S, Cordelieres FP (2006). A guided tour into subcellular colocalization analysis in light microscopy. J Microsc 224, 213–232.

Boucrot E, Kirchhausen T (2007). Endosomal recycling controls plasma membrane area during mitosis. Proc Natl Acad Sci USA 104, 7939–7944.

Brill JA, Wong R, Wilde A (2011). Phosphoinositide function in cytokinesis. Curr Biol 21, R930–934.

Echard A (2012). Phosphoinositides and cytokinesis: the "PIP" of the iceberg. Cytoskeleton 69, 893–912.

Furse S, Brooks NJ, Seddon AM, Woscholski R, Templer RH, Tate EW, Gaffney PRJ, Ces O (2012). Lipid membrane curvature induced by distearoyl phosphatidylinositol 4-phosphate. Soft Matter 8, 3090–3093.

Galione A, Chuang KT (2012). Pyridine nucleotide metabolites and calcium release from intracellular stores. Adv Exp Med Biol 740, 305–323.

Galione A, Morgan AJ, Arredouani A, Davis LC, Rietdorf K, Ruas M, Parrington J (2010). NAADP as an intracellular messenger regulating lysosomal calcium-release channels. Biochem Soc Trans 38, 1424–1431.

Godi A, Pertile P, Meyers R, Marra P, Di Tullio G, Iurisci C, Luini A, Corda D, De Matteis MA (1999). ARF mediates recruitment of PtdIns-4-OH kinase-beta and stimulates synthesis of PtdIns(4,5)P2 on the Golgi complex. Nat Cell Biol 1, 280–287.

Handley MT, Lian LY, Haynes LP, Burgoyne RD (2010). Structural and functional deficits in a neuronal calcium sensor-1 mutant identified in a case of autistic spectrum disorder. PLoS One 5, e10534.

Haynes LP, Thomas GM, Burgoyne RD (2005). Interaction of neuronal calcium sensor-1 and ADP-ribosylation factor 1 allows bidirectional control of phosphatidylinositol 4-kinase beta and trans-Golgi network-plasma membrane traffic. J Biol Chem 280, 6047–6054.

Holt OJ, Gallo F, Griffiths GM (2006). Regulating secretory lysosomes. J Biochem 140, 7–12.

Lenoir M, Overduin M (2013). PtdIns(4)P signalling and recognition systems. Adv Exp Med Biol 991, 59–83.

Liu Y, Boukhelifa M, Tribble E, Morin-Kensicki E, Uetrecht A, Bear JE, Bankaitis VA (2008). The Sac1 phosphoinositide phosphatase regulates Golgi membrane morphology and mitotic spindle organization in mammals. Mol Biol Cell 19, 3080–3096.

Luzio JP, Bright NA, Pryor PR (2007a). The role of calcium and other ions in sorting and delivery in the late endocytic pathway. Biochem Soc Trans 35, 1088–1091.

Luzio JP, Pryor PR, Bright NA (2007b). Lysosomes: fusion and function. Nat Rev Mol Cell Biol 8, 622–632.

Ly DH, Lockhart DJ, Lerner RA, Schultz PG (2000). Mitotic misregulation and human aging. Science 287, 2486–2492.

Matteoni R, Kreis TE (1987). Translocation and clustering of endosomes and lysosomes depends on microtubules. J Cell Biol 105, 1253–1265.

McCue HV, Burgoyne RD, Haynes LP (2009). Membrane targeting of the EF-hand containing calcium-sensing proteins CaBP7 and CaBP8. Biochem Biophys Res Commun 380, 825–831.

McCue HV, Burgoyne RD, Haynes LP (2011). Determination of the membrane topology of the small EF-Hand Ca^{2+}-sensing proteins CaBP7 and CaBP8. PLoS One 6, e17853.

McCue HV, Haynes LP, Burgoyne RD (2010a). Bioinformatic analysis of CaBP/calneuron proteins reveals a family of highly conserved vertebrate Ca2+-binding proteins. BMC Res Notes 3, 118.

McCue HV, Haynes LP, Burgoyne RD (2010b). The diversity of calcium sensor proteins in the regulation of neuronal function. Cold Spring Harb Perspect Biol 2, a004085.

McCue HV, Patel P, Herbert AP, Lian LY, Burgoyne RD, Haynes LP (2012). Solution NMR structure of the Ca2+-bound N-terminal domain of CaBP7: a regulator of Golgi trafficking. J Biol Chem 287, 38231–38243.

McCue HV, Wardyn JD, Burgoyne RD, Haynes LP (2013). Generation and characterization of a lysosomally targeted, genetically encoded Ca2+-sensor. Biochem J 449, 449–457.

McNeil PL, Kirchhausen T (2005). An emergency response team for membrane repair. Nat Rev Mol Cell Biol 6, 499–505.

Mierzwa B, Gerlich DW (2014). Cytokinetic abscission: molecular mechanisms and temporal control. Dev Cell 31, 525–538.

Mikhaylova M, Reddy PP, Munsch T, Landgraf P, Suman SK, Smalla KH, Gundelfinger ED, Sharma Y, Kreutz MR (2009). Calneurons provide a calcium threshold for trans-Golgi network to plasma membrane trafficking. Proc Natl Acad Sci USA 106, 9093–9098.

Miller AL, Fluck RA, McLaughlin JA, Jaffe LF (1993). Calcium buffer injections inhibit cytokinesis in Xenopus eggs. J Cell Sci 106, 523–534.

Neumann B, Walter T, Heriche JK, Bulkescher J, Erfle H, Conrad C, Rogers P, Poser I, Held M, Liebel U, et al. (2010). Phenotypic profiling of the human genome by time-lapse microscopy reveals cell division genes. Nature 464, 721–727.

Pfau SJ, Amon A (2012). Chromosomal instability and aneuploidy in cancer: from yeast to man. EMBO Rep 13, 515–527.

Polevoy G, Wei HC, Wong R, Szentpetery Z, Kim YJ, Goldbach P, Steinbach SK, Balla T, Brill JA (2009). Dual roles for the Drosophila PI 4-kinase four wheel drive in localizing Rab11 during cytokinesis. J Cell Biol 187, 847–858.

Ricke RM, van Deursen JM (2013). Aneuploidy in health, disease, and aging. J Cell Biol 201, 11–21.

Sridhar S, Patel B, Aphkhazava D, Macian F, Santambrogio L, Shields D, Cuervo AM (2013). The lipid kinase PI4KIIIbeta preserves lysosomal identity. EMBO J 32, 324–339.

Walch-Solimena C, Novick P (1999). The yeast phosphatidylinositol-4-OH kinase pik1 regulates secretion at the Golgi. Nat Cell Biol 1, 523–525.

Whitaker M (2006). Calcium microdomains and cell cycle control. Cell Calcium 40, 585–592.

Zhao X, Varnai P, Tuymetova G, Balla A, Toth ZE, Oker-Blom C, Roder J, Jeromin A, Balla T (2001). Interaction of neuronal calcium sensor-1 (NCS-1) with phosphatidylinositol 4-kinase beta stimulates lipid kinase activity and affects membrane trafficking in COS-7 cells. J Biol Chem 276, 40183–40189.